Speed Control for Doubly-Fed Induction Motors With and Without Current Feedback

Marc Bodson, *IEEE Fellow*

Abstract—The paper presents a method to control the speed of doubly-fed induction motors. The motivation lies in the possible use of such motors for hybrid electric propulsion. The stator of the motor is assumed to be supplied by three-phase voltages with frequency and magnitude that may vary. The rotor is supplied by a bi-directional converter. Two versions of the algorithm are presented. The first version does not rely on inner current loops, but instead commands directly the voltages applied to the rotor. These voltages are computed using an open-loop controller for torque and for stator reactive power, which is augmented to follow a speed reference profile. The second version uses stator and rotor current measurements to ensure tracking and limiting of the rotor currents. All the parameters of the control systems can be computed based on estimates of the machine parameters together with a desired time constant of the speed response. The alignment of an incremental encoder is integrated in the initialization of the algorithm. Practical implementation and testing are performed easily and rapidly. Experiments performed on a small-scale laboratory testbed show very good tracking performance of a speed profile in tests involving one motor, as well as two motors on a single three-phase supply. Improved current limiting is observed with the version incorporating current feedback.

Keywords: electric motors, electric propulsion, doubly-fed induction machines, complex vectors, vector control

I. INTRODUCTION

Historically, doubly-fed induction motors (also called wound-rotor induction motors) found limited use as alternatives to squirrel-cage induction motors supplied directly by the grid. With their rotor windings connected to external resistors, their characteristics are identical to squirrel-cage machines, but the addition of resistance to the rotor at start-up yields reduced start-up currents and increased torque. In steady-state, the rotor resistance can be reduced to increase the efficiency of the machine, or adjusted to vary the speed over a limited range. With the advent of power electronics, resistors were replaced by a rectifier combined with a DC/AC converter for the regeneration of the rotor-side power. Controlling the amount of regenerated power is then similar to varying the rotor resistance, and is a means of controlling the speed [1].

The use of doubly-fed induction machines expanded considerably through their use as generators for wind power. The earlier combination of rectifier + DC/AC converter was replaced by a bi-directional AC/AC converter. Variable speed generation was possible through the control of the magnitude, frequency, and phase of the rotor currents. A significant advantage of doubly-fed induction machines is that the power flowing through the rotor is a fraction of the power flowing directly from the stator to the grid. Neglecting losses, the

M. Bodson is with the Department of Electrical and Computer Engineering, University of Utah, 50 S Central Campus Dr, Rm 2110, Salt Lake City, UT 84112, U.S.A. (e-mail: bodson@eng.utah.edu).

percentage of power is equal to the percentage of speed variation around the synchronous speed. In a generator, the power produced on the stator is transmitted to the grid without conversion, or conversion losses. Other generators either have very small speed range (low-power grid-tied squirrel-cage induction generators) or require full power AC/AC conversion. Doubly-fed induction generators also allow for the independent control of the active and reactive powers using the rotor currents [2]-[4].

The advantages of doubly-fed induction generators carry over to doubly-fed induction motors, but have not been explored to the same extent. The possibility has been studied in electric propulsion for land [5], marine [6], and aircraft propulsion [7]. Two main approaches have been followed for motor control. The first approach adopts the same strategy as the one used for doubly-fed induction generators, with a single converter controlling the rotor currents and with the stator connected directly to the grid. Operational procedures and benefits are similar, although not identical to those for doubly-fed induction generators. Examples of studies using this approach include [8]-[15], and the present paper. The second approach consists in having two converters: one for the control of the rotor currents and one for the stator currents. An interesting option consists in having converters rated each at 50% of the total power. Then, equal power is transmitted to the stator and rotor windings, and with equal frequencies on the stator and on the rotor (however, in reverse sequence on the rotor). Examples of this approach include [5] [6] [16] -[18]

Most control algorithms for doubly-fed induction machines are based on some form of field-oriented control, similar to the methods used for squirrel-cage machines. The problem is somewhat simpler when two converters are used, since both the stator and the rotors currents can be controlled. For example, the controller can regulate the torque, the flux level, the stator frequency and the slip (or ratio of stator to rotor power). With only one converter and a fixed stator voltage and frequency, the problem becomes more comparable to the control of squirrel-cage machines, although the fluxes can be estimated more easily through measurements of the stator and rotor currents. The flux magnitude is also mostly determined by the stator voltages. In this case, it is typical to control the active and reactive powers, or the torque and the reactive power.

In almost all algorithms, it is assumed that an inner loop regulates the currents. This regulation is achieved with switched-mode amplifiers (hysteresis) or using a model-based control law derived from the known dynamics of the motor. The complexity of the system makes it difficult to prove

stability, although [11] presents such a proof using Lyapunov arguments. Sensorless control is sometimes considered, and usually achieved through simple integration of the estimated fluxes [15] [18].

A difficulty with the single converter option is the start-up of the motor. If a connection to the grid is attempted at standstill with minimal transients, the required rotor voltages may exceed the converter capabilities. Therefore, various start-up methods have been proposed. Some papers consider having a transformer on the stator [14], while others consider having a transformer on the rotor [10]. Other proposed solutions start the motor as a squirrel-cage motor, with switches to return to the normal configuration at an appropriate time. References [1] and [15] start the motor with the rotor short-circuited or with external resistors. The stator is connected to the grid and the rotor converter takes over once a certain speed is reached. Conversely, reference [13] starts the motor with the converter engaged and the stator short-circuited, then connects the stator to the grid once a certain speed is reached. Reference [8] does the same with a DC source connected to the stator initially. These multiple solutions highlight the multiple ways in which the doubly-fed induction motor can be operated.

It is also interesting to note the significant body of work dedicated to brushless doubly-fed induction machines. This denomination includes machines of significantly different construction, but with the advantage of not requiring slip rings to transfer power to the rotor windings. Other limitations surface however, and resolving them has been the subject of much research. One category of brushless doubly-fed machines is of the reluctance type [19] [20], whose dynamics are identical to those of doubly-fed induction motors (as opposed to synchronous reluctance motors). Another category consists of two doubly-fed induction motors placed on the same shaft and with their rotor windings in parallel but in reverse sequence [21]. Various approaches have been followed to integrate the two machines into a single core. The dynamics of these motors are not identical to those of doubly-fed induction motors, but it is likely that they could be controlled using techniques similar to those presented in this paper.

This paper's motivation originates from a goal to use doubly-fed induction machines for hybrid electric propulsion [7]. The benefits of such motors extend to land and marine propulsion as well, and possibly new applications to be developed. A single converter configuration is assumed. The paper proposes a speed and reactive power control algorithm with two options: with and without current sensors. In both cases, a complex variable representation results in a description of the algorithm with few equations. Importantly, all the controller parameters can be determined a priori from estimates of the system parameters and from a reasonable choice of controller bandwidth. The simplest option without current feedback makes it possible to rapidly implement a controller for speed control of doubly-fed induction motors. The second option uses stator and rotor current sensors to ensure tighter rotor current regulation and limiting. Even then, the first option can be useful as an intermediate step to test the integrity of the digital control architecture, or to continue operation in case of sensor failures. The computational needs of the first option

are also low, and stability can be proved relatively easily.

The paper does not discuss start-up methods. In the electric propulsion application envisioned, the stator is supplied by an AC generator (possibly a doubly-fed induction machine as well), and the stator voltage can be reduced at start-up through excitation control on the generator. Otherwise, one of several methods proposed in the literature and mentioned earlier can be used for start-up.

II. DOUBLY-FED INDUCTION MACHINE

A. Machine structure

Fig. 1 shows a schematic representation of a doubly-fed induction machine (DFIM), with three stator windings and three rotor windings. The voltages applied to the stator windings are denoted v_{SA}, v_{SB}, v_{SC}, while the currents flowing in the windings are denoted i_{SA}, i_{SB}, i_{SC} (with the sign convention as shown on the figure). Similarly, the voltages applied to the rotor windings are denoted v_{RX}, v_{RY}, v_{RZ}, while the currents flowing into the windings are denoted i_{RX}, i_{RY}, i_{RZ}. The position of the rotor is determined by the angle θ, which is the angle between the stator winding A and the rotor winding X. The figure shows a motor with one pole pair, but the analysis of the paper applies to an arbitrary number of pole pairs n_P.
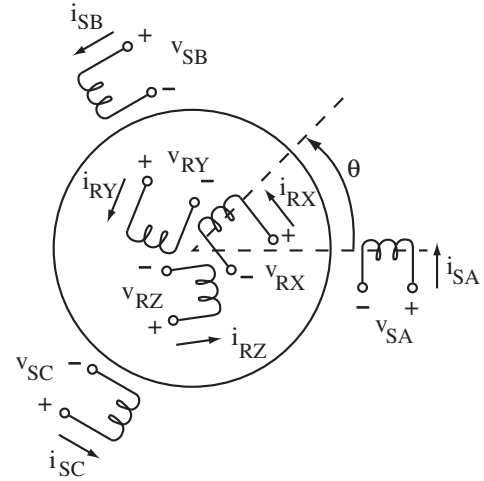

Fig. 1. Doubly-fed induction machine

B. Three-phase to complex transformation

We consider a *three-phase to complex transformation (3-c transformation)* defined by

$$v_S = \sqrt{\frac{2}{3}}\, e^{-j\theta_e}$$

$$\begin{pmatrix} 1 & -1/2 + j\sqrt{3}/2 & -1/2 - j\sqrt{3}/2 \end{pmatrix} \begin{pmatrix} v_{SA} \\ v_{SB} \\ v_{SC} \end{pmatrix} \quad (1)$$

where θ_e is an arbitrary angle and v_S is a complex but scalar signal. The transformation is the combination of three operations: a three-phase to two-phase transformation, the grouping of the two-phase variables into a single complex

variable, and the counterclockwise rotation of the resulting complex variable by the angle θ_e. The transformation to complex variables has been used to a lesser extent than the other two operations, despite being proposed decades ago [22] [23]. The complex model not only simplifies the notation and the derivations, but also enables alternative stability analysis and control design methods [21] [24] [25].

The stator currents are transformed using the same 3-c transformation to produce the complex variable i_S. If the angle θ_e is chosen such that v_S is real, the transformation corresponds to the use of a *stator voltage-oriented reference frame*, which is common in the analysis of doubly-fed induction generators. The components of the current vector in such a frame are typically denoted i_{SD}, i_{SQ}, and the complex variable i_S is then $i_S = i_{SD} + ji_{SQ}$.

If $v_{SA} + v_{SB} + v_{SC} = 0$ (Y or Δ connection), the inverse of the 3-c transformation (or *inverse 3-c*) is given by

$$
\begin{pmatrix} v_{SA} \\ v_{SB} \\ v_{SC} \end{pmatrix} = \sqrt{\frac{2}{3}} \begin{pmatrix} 1 & 0 \\ -1/2 & \sqrt{3}/2 \\ -1/2 & -\sqrt{3}/2 \end{pmatrix}
\begin{pmatrix} \mathrm{Re}(v_S e^{j\theta_e}) \\ \mathrm{Im}(v_S e^{j\theta_e}) \end{pmatrix} \tag{2}
$$

For the rotor variables, the 3-c transformation includes an additional term related to the rotor angle θ defined earlier, with

$$
v_R = \sqrt{\frac{2}{3}} \, e^{-j(\theta_e - n_P \theta)}
$$
$$
\begin{pmatrix} 1 & -1/2 + j\sqrt{3}/2 & -1/2 - j\sqrt{3}/2 \end{pmatrix} \begin{pmatrix} v_{RX} \\ v_{RY} \\ v_{RZ} \end{pmatrix} \tag{3}
$$

where n_P is the number of pole pairs. The angle $n_P\theta$ is inserted to refer the rotor variables to the stator frame of reference. Assuming that $v_{RX} + v_{RY} + v_{RZ} = 0$, the inverse of the transformation is

$$
\begin{pmatrix} v_{RX} \\ v_{RY} \\ v_{RZ} \end{pmatrix} = \sqrt{\frac{2}{3}} \begin{pmatrix} 1 & 0 \\ -1/2 & \sqrt{3}/2 \\ -1/2 & -\sqrt{3}/2 \end{pmatrix}
\begin{pmatrix} \mathrm{Re}(v_R e^{j(\theta_e - n_P\theta)}) \\ \mathrm{Im}(v_R e^{j(\theta_e - n_P\theta)}) \end{pmatrix} \tag{4}
$$

The leading coefficient of the three-phase to complex transformation is one of three options found in the literature. It preserves the definition of power and is used in [26], for example. It can be shown that, with a Y or Δ connection,

$$
v_S i_S^* = P_S + jQ_S \tag{5}
$$

where P_S and Q_S are the (total) instantaneous active and reactive powers absorbed by the stator windings.

Consider the steady-state operation with V_{pk} and I_{pk} being the peak values of the stator voltages and currents, and φ being the power factor, so that

$$
v_{SA} = V_{pk}\cos(\theta_e), \;\; i_{SA} = I_{pk}\cos(\theta_e - \varphi) \tag{6}
$$

The voltages and currents in phases B and C are the same but shifted by $2\pi/3$ and $-2\pi/3$. Then

$$
P_S + jQ_S = \frac{3}{2} V_{pk} I_{pk} e^{j\varphi} \tag{7}
$$

Further, the complex variables satisfy

$$
v_S = \sqrt{3/2}V_{pk}, \;\; i_S = \sqrt{3/2}I_{pk}e^{-j\varphi} \tag{8}
$$

In other words, v_S and i_S are phasors for v_{SA} and i_{SA} in steady-state (as well as v_{SB}, v_{SC}, i_{SB}, i_{SC}, with phase shifts of $\pm 2\pi/3$). The multiplicative factor of $\sqrt{3/2}$ can be removed by adjusting the leading coefficient of the 3-c transformation, but then a coefficient $3/2$ has to be inserted in the power relationship (5).

C. Model of the DFIM and steady-state operation

The model of a doubly-fed induction motor in the complex coordinates is

$$
\begin{aligned}
L_S \frac{di_S}{dt} + M\frac{di_R}{dt} &= v_S - R_S i_S \\
&\quad - j\omega_e(L_S i_S + M i_R) \\
M\frac{di_S}{dt} + L_R\frac{di_R}{dt} &= v_R - R_R i_R \\
&\quad - j(\omega_e - n_P\omega)(L_R i_R + M i_S) \\
\tau_e &= n_P M \,\mathrm{Im}(i_S i_R^*) \tag{9}
\end{aligned}
$$

where $\omega_e = d\theta_e/dt$, $\omega = d\theta/dt$, and τ_e is the torque of the motor. R_S and R_R are the stator and rotor winding resistances, L_S and L_R are the stator and rotor winding inductances, and M is the mutual inductance between stator and rotor windings when aligned.

Assuming that ω and ω_e are constant (or slowly-varying, in practice), the Laplace transform can be applied to the model of the system, resulting in

$$
\begin{pmatrix} sL_S + Z_S & sM + Z_{MS} \\ sM + Z_{MR} & sL_R + Z_R \end{pmatrix} \begin{pmatrix} i_S \\ i_R \end{pmatrix} = \begin{pmatrix} v_S \\ v_R \end{pmatrix} \tag{10}
$$

where

$$
\begin{aligned}
Z_S &= R_S + j\omega_e L_S & Z_{MS} &= j\omega_e M \\
Z_R &= R_R + j(\omega_e - n_P\omega)L_R & Z_{MR} &= j(\omega_e - n_P\omega)M
\end{aligned} \tag{11}
$$

Therefore

$$
\begin{pmatrix} i_S \\ i_R \end{pmatrix} = \frac{1}{\Delta Z(s)} \begin{pmatrix} sL_R + Z_R & -sM - Z_{MS} \\ -sM - Z_{MR} & sL_S + Z_S \end{pmatrix} \begin{pmatrix} v_S \\ v_R \end{pmatrix} \tag{12}
$$

where

$$
\Delta Z(s) = (sL_S + Z_S)(sL_R + Z_R) - (sM + Z_{MR})(sM + Z_{MS}) \tag{13}
$$

The poles of the system are given by the two roots of the polynomial $\Delta Z(s)$, and the transfer function from v_R to i_S is given by

$$
\frac{i_S}{v_R} = \frac{-sM - Z_{MS}}{\Delta Z(s)} \tag{14}
$$

Control using the complex model can be pursued successfully, with an example using pole placement for doubly-fed

induction generators found in [27] [28] and an example using a root-locus method for three-phase inverters found in [29]. The poles of the system with real parameters are the union of the poles of the system with complex parameters, together with their complex conjugates. Therefore, the stability properties of both systems are identical (for more details on the theory, see [24]). For example, the complex model makes it possible to prove the following fact:

Fact: the electrical model of the doubly-fed induction machine is stable at constant speed for all possible values of the parameters, including the speed of the motor.

Proof of the fact: the roots of the characteristic polynomial $\Delta Z(s)$ are equal to the roots of $\Delta Z(s - j\omega_e)$ shifted by $j\omega_e$. Therefore, the system is stable if and only if the roots of $\Delta Z(s - j\omega_e)$ are in the open left-half plane. The polynomial is equal to

$$\Delta Z(s - j\omega_e) = a_0 s^2 + (a_1 + jb_1)s + a_2 + jb_2 \quad (15)$$

where

$$a_0 = L_S L_R - M^2, \quad a_1 = L_S R_R + L_R R_S, \quad a_2 = R_S R_R$$
$$b_1 = -n_P \omega (L_S L_R - M^2), \quad b_2 = -n_P \omega L_R R_S \quad (16)$$

Using the method of [30], the roots are in the open left-half plane if and only if

$$a_0 > 0, \quad a_1 > 0, \quad \Delta_2 = \begin{vmatrix} a_1 & 0 & -b_2 \\ a_0 & a_2 & -b_1 \\ 0 & b_2 & a_1 \end{vmatrix} > 0 \quad (17)$$

The coefficient $a_0 = \sigma L_S L_R$ where σ is the leakage factor. Therefore, for positive machine parameters, $a_0 > 0$, $a_1 > 0$, while the determinant is equal to

$$\begin{aligned} \Delta_2 &= (L_S R_R + L_R R_S)^2 R_S R_R \\ &\quad + (L_S R_R + L_R R_S)(n_P \omega)^2 (\sigma L_S L_R)(L_R R_S) \\ &\quad - (\sigma L_S L_R)(n_P \omega)^2 (L_R R_S)^2 \\ &= (L_S R_R + L_R R_S)^2 R_S R_R \\ &\quad + (L_S L_R R_S R_R)(n_P \omega)^2 (\sigma L_S L_R) \end{aligned} \quad (18)$$

With $\Delta_2 > 0$, the proof is completed.

III. CONTROL OF A DOUBLY-FED INDUCTION MOTOR

A. Control of torque and reactive power with voltage command

Steady-state operation is defined by sinusoidal voltages and currents of frequency ω_e (for the rotor, the frequency of the physical variables is actually $\omega_e - n_P \omega$). Because the electrical system is stable, convergence to a steady-state can be assumed for constant (or nearly constant, in practice) variables. In steady-state, the variables v_S, i_S, v_R, and i_R satisfy

$$\begin{aligned} v_S &= Z_S i_S + Z_{MS} i_R \\ v_R &= Z_R i_R + Z_{MR} i_S \end{aligned} \quad (19)$$

Therefore, the rotor voltage needed to achieve a certain current i_S is found to be

$$v_R = \frac{Z_R}{Z_{MS}} v_S - \left(\frac{Z_S Z_R - Z_{MS} Z_{MR}}{Z_{MS}} \right) i_S \quad (20)$$

Let θ_e chosen such that v_S is real (stator voltage alignment). Then, using (5) and (9)

$$\begin{aligned} v_S \operatorname{Re}(i_S) &= R_S \left(\operatorname{Re}(i_S)^2 + \operatorname{Im}(i_S)^2 \right) + \frac{\omega_e \tau_e}{n_P} \\ v_S \operatorname{Im}(i_S) &= -Q_S \end{aligned} \quad (21)$$

Solving for $\operatorname{Re}(i_S)$ and $\operatorname{Im}(i_S)$, one finds that

$$i_S = \frac{v_S}{2R_S} - \sqrt{\left(\frac{v_S}{2R_S} \right)^2 - \left(\frac{\omega_e \tau_e}{n_P R_S} + \frac{Q_S^2}{v_S^2} \right)} - j\frac{Q_S}{v_S} \quad (22)$$

In the solution of the quadratic equation for $\operatorname{Re}(i_S)$, the minus sign was chosen so that $i_S = 0$ when $\tau_e = 0$ and $Q_S = 0$.

Combining (20) and (22) gives the rotor voltage needed to achieve a desired torque τ_{COM} and a desired stator reactive power Q_{COM} (absorbed), based on the intermediate stator current command $i_{S,COM}$. For example, with $Q_{COM} = 0$, the control law is

$$v_R = \frac{Z_R}{Z_{MS}} v_S - \left(\frac{Z_S Z_R - Z_{MS} Z_{MR}}{Z_{MS}} \right) i_{S,COM} \quad (23)$$

with

$$i_{S,COM} = \frac{v_S}{2R_S} - \sqrt{\left(\frac{v_S}{2R_S} \right)^2 - \left(\frac{\omega_e \tau_{COM}}{n_P R_S} \right)} \quad (24)$$

The result is an open-loop control algorithm that, in theory, provides a decoupled response with unity gain from torque command to actual torque. The unity gain concerns the steady-state response, *i.e*, the DC gain of the system at $s = 0$. The transient response is affected by the poles of the system that are given by the roots of (13). However, as shown in the fact above, the poles are known to be stable. In practice, they are also associated with small time constants.

B. Closed-loop control of velocity

Fig. 2 shows the implementation of a velocity control algorithm using the open-loop controller for torque. The doubly-fed induction motor is fed on the rotor by a voltage source converter (VSC). The torque control block implements (23), (24). Speed control can be achieved with a proportional-integral control algorithm

$$\begin{aligned} \tau_{COM} &= K_F K_P \, \omega_{REF} - K_P \, \omega + K_I \, e_I \\ \frac{de_I}{dt} &= \omega_{REF} - \omega \quad \text{if } |\tau_{COM}| \leqslant \tau_{LIM} \\ &= 0 \quad \quad \quad \text{otherwise} \end{aligned} \quad (25)$$

where ω_{REF} is the reference value for the speed. In the algorithm, K_P is a proportional gain, K_I is an integral gain, K_F is a feedforward gain applied to shift the location of the closed-loop zero and avoid overshoot in the response, and τ_{LIM} is a torque limit applied to stay within constraints and avoid integrator wind-up (more details on this issue below).

For the selection of the PI gains, assume that the torque tracks the command and that the dynamics of the motor are adequately characterized by the standard mechanical equation

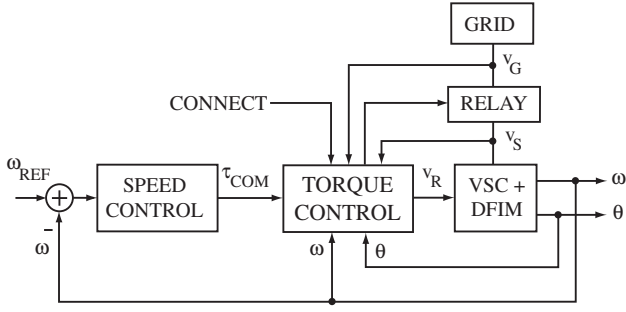$$J\frac{d\omega}{dt} = \tau_{COM} - \tau_L \quad (26)$$

Fig. 2. Control of motor velocity

where J is the inertia of the motor and load, and τ_L is the non-inertial component of the load torque. The load torque is treated as a disturbance for analysis. The closed-loop dynamics of the speed control loop are given by the roots of

$$Js^2 + K_P s + K_I = 0 \qquad (27)$$

Both poles of the velocity loop can be set at some desired value $s = -a_{D,VEL}$ by letting $K_P = 2a_{D,VEL} J$ and $K_I = a_{D,VEL}^2 J$. Generally, a value of $K_F = 2/3$ yields a fast response without overshoot. In this manner, all the parameters of the proposed control algorithm can be specified *a priori*.

Note that the integrator of the PI algorithm not only ensures the tracking of a velocity command in steady-state, but also reduces the effect of small errors in the open-loop tracking of the torque command. A PI control loop can also be added for the closed-loop control of the reactive power. In that case, the parameters of the controller can be set assuming a unity response from reactive power command to reactive power.

C. Synchronization

Fig. 2 shows a relay that is used to connect the motor to the grid at start-up. The procedure is similar to the synchronization of a synchronous generator to the grid, but is simpler and possible at arbitrary speed (in particular, zero speed at start-up). The connection of the open stator to the grid corresponds to setting $i_{S,COM} = 0$ in (23), giving the rotor voltage needed to match the grid voltage v_G as $v_R = (Z_R/Z_{MS}) v_G$. With the stator voltage orientation, the frequency of the stator voltages and of the grid voltages are matched automatically. In theory, the magnitude and phase are also matched, but small modelling errors create mismatch in magnitude and phase. If an incremental encoder is used without alignment, the phase error can be very large. By inserting two adjustable parameters m_{adj} and θ_{adj} in a modified expression for the rotor voltage

$$v_R = m_{adj}\, e^{j\theta_{adj}} \frac{Z_R}{Z_{MS}} v_G \qquad (28)$$

the synchronization procedure provides an opportunity to align the encoder as well as compensate for small errors. The angular adjustment is also applied to the second term of (23) after the motor is connected.

D. Torque and reactive power limits

Limits can be placed in the control law to ensure that the constraints are satisfied. For simplicity, we consider two special cases where limits can be computed with relatively simple analytic expressions.

Case 1: consider the case with $Q_{COM} = 0$. Then, both v_S and $i_{S,COM}$ are real. For the square root in (24) to be well-defined, one needs

$$\frac{\omega_e \tau_{COM}}{n_p R_S} \leqslant \left(\frac{v_S}{2R_S}\right)^2 \qquad (29)$$

which implies a limit on the torque

$$\tau_{COM} \leqslant \tau_{MAX,1} \triangleq \frac{n_P}{\omega_e} \frac{v_S^2}{4R_S} \qquad (30)$$

From (21), one has

$$v_S i_S = R_S i_S^2 + \frac{\omega_e \tau_e}{n_P} \qquad (31)$$

so that a limit on the current $|i_S| \leqslant i_{S,MAX}$ implies a limit on the torque

$$\tau_{COM} \leqslant \tau_{MAX,2} \triangleq \frac{n_P}{\omega_e} \left(v_S i_{S,MAX} - R_S i_{S,MAX}^2\right) \quad (32)$$

Finally, the rotor current is given by

$$i_R = -\frac{L_S}{M} i_S - j\frac{v_S - R_S i_S}{\omega_e M} \qquad (33)$$

so that

$$|i_R|^2 - i_{R,MAX}^2 = a_1 i_S^2 - 2a_2 i_S - a_3 \qquad (34)$$

where

$$a_1 = \frac{R_S^2 + \omega_e^2 L_S^2}{\omega_e^2 M^2}, \quad a_2 = \frac{R_S v_S}{\omega_e^2 M^2}, \quad a_3 = i_{R,MAX}^2 - \frac{v_S^2}{\omega_e^2 M^2} \qquad (35)$$

Then $|i_R| \leqslant i_{R,MAX}$ if

$$i_S \leqslant i_{S,RMAX} \triangleq \left(a_2 + \sqrt{a_2^2 + a_1 a_3}\right)/a_1 \qquad (36)$$

This new limit on the stator current due to the rotor current limit implies a third limit on the torque.

$$\tau_{COM} \leqslant \tau_{MAX,3} \triangleq \frac{n_P}{\omega_e} \left(v_S i_{S,RMAX} - R_S i_{S,RMAX}^2\right) \qquad (37)$$

Note that the limits were computed for positive (motoring) torque. Limits for negative torque can be computed similarly, but are slightly different.

Example: consider a small motor with parameters $R_S = 0.66\ \Omega$, $R_R = 0.94\ \Omega$, $L_S = 13.1$ mH, $L_R = 9.8$ mH, $M = 9.7$ mH, $n_P = 2$. Assume that the supply voltage is 11.1 V_{pk} line-neutral, and that the stator and rotor line currents are limited to 6 A_{pk}. Converting the values to complex equivalent variables using (8), one finds $v_S = 13.6$ V, $i_{S,MAX} = 7.35$ A, and $i_{R,MAX} = 7.35$ A. The limits on the torque are then computed to be $\tau_{MAX,1} = 0.371$ N.m, $\tau_{MAX,2} = 0.341$ N.m, $\tau_{MAX,3} = 0.274$ N.m. Therefore, the torque limit is due to the rotor current limit and is $\tau_{LIM} = 0.274$ N.m.

Case 2: consider the case where $R_S = 0$. This approximation is appropriate for large machines. This case can be solved

without assuming $Q_{COM} = 0$. Equation (21) with $R_S = 0$ gives

$$i_S = \frac{\omega_e \tau_e}{v_S n_P} - j \frac{Q_S}{v_S} \qquad (38)$$

The open-loop control algorithm is simply

$$v_R = \frac{Z_R}{Z_{MS}} v_S - \left(\frac{Z_S Z_R - Z_{MS} Z_{MR}}{Z_{MS}} \right) \cdot \\ \left(\frac{\omega_e \tau_{COM}}{v_S n_P} - j \frac{Q_{COM}}{v_S} \right) \qquad (39)$$

The first torque limit disappears in this case. With a limit on the stator current $|i_S| \leqslant i_{S,MAX}$, the torque and reactive power are jointly restricted by the quadratic constraint

$$\left(\frac{\omega_e \tau_{COM}}{v_S n_P} \right)^2 + \left(\frac{Q_{COM}}{v_S} \right)^2 \leqslant i_{S,MAX}^2 \qquad (40)$$

From (33) and (38), the rotor current is given by

$$i_R = -\frac{L_S}{M} \frac{\omega_e \tau_e}{v_S n_P} - j \left(\frac{v_S}{\omega_e M} - \frac{L_S}{M} \frac{Q_S}{v_S} \right) \qquad (41)$$

With a limit on the rotor current $|i_R| \leqslant i_{R,MAX}$, the torque and reactive power are restricted by a second constraint

$$\left(\frac{L_S}{M} \frac{\omega_e \tau_{COM}}{v_S n_P} \right)^2 + \left(\frac{v_S}{\omega_e M} - \frac{L_S}{M} \frac{Q_{COM}}{v_S} \right)^2 \leqslant i_{R,MAX}^2 \qquad (42)$$

This inequality shows that a higher torque can be reached with $Q_{COM} > 0$, and maximum torque is obtained when $Q_{COM} = v_S^2/(\omega_e L_S)$. This means that all the magnetizing current of the motor is provided by the supply connected to the stator instead of the rotor converter. For given Q_{COM}, (40) and (42) yield torque limits $\tau_{MAX,2}$ and $\tau_{MAX,3}$, from which τ_{LIM} can be deduced.

E. Current control loop

Although limits can be applied to the torque and reactive power commands to ensure that currents stay within their limits, the effectiveness of the limiting depends on the accuracy of the electrical model and of its parameters. Operation must also be such that the steady-state approximation is valid. In order to protect the rotor-side converter, tighter current regulation and limiting may be desired. The result can be achieved using an inner current control loop and assuming the availability of current sensors. Current control schemes have been developed extensively for cage rotor induction machines, including with a complex representation of the system comparable to the one used in this paper [31] [32]. A current control algorithm is proposed here using a complex representation and inspired from algorithms developed for cage rotor machines [33]. As the DFIM is controlled from the rotor, the roles of the stator and rotor are reversed compared to the cage rotor case. The problem is at the same time simpler and more complicated: simpler because the flux can be computed from measurements of the rotor and stator currents (as opposed to using a flux estimator), and more complicated because the stator is connected to a voltage source (as opposed to short-circuited windings).

Using the steady-state relationship (19) and the definitions (11), the rotor current needed to achieve a certain current $i_{S,COM}$ is given by

$$i_{R,COM} = \frac{v_S - Z_S i_{S,COM}}{Z_{MS}} \qquad (43)$$

Therefore, the torque control algorithm composed (23) and (24) is replaced by (24) and (43), together with a feedback control law for the rotor currents.

Using the definitions (11), the first two equations of (9) can be written as

$$L_S \frac{di_S}{dt} + M \frac{di_R}{dt} = v_S - Z_S i_S - Z_{MS} i_R$$
$$M \frac{di_S}{dt} + L_R \frac{di_R}{dt} = v_R - Z_R i_R - Z_{MR} i_S \qquad (44)$$

Solving for di_R/dt gives

$$\frac{di_R}{dt} = \frac{1}{\sigma L_R} (v_R - u_R) \qquad (45)$$

where $\sigma = 1 - M^2/(L_S L_R)$ and

$$u_R = Z_R i_R + Z_{MR} i_S + \frac{M}{L_S} (v_S - Z_S i_S - Z_{MS} i_R) \qquad (46)$$

The control law for the rotor current is chosen to be

$$v_R = u_R - R_T i_R + K_{P,C} (i_{R,COM} - i_R) \\ + K_{I,C} \int (i_{R,COM} - i_R) dt \qquad (47)$$

where $i_{R,COM}$ is the desired value set for the rotor current (43), and R_T, $K_{P,C}$, $K_{I,C}$ are controller parameters to be determined.

In the Laplace domain, the transfer function from the rotor current command $i_{R,COM}$ to the rotor current i_R is

$$\frac{i_R}{i_{R,COM}} = \frac{K_{P,C} s + K_{I,C}}{\sigma L_R s^2 + (K_{P,C} + R_T) s + K_{I,C}} \qquad (48)$$

Similarly to [33], we set

$$K_{P,C} = \sigma L_R a_{D,CUR}, \quad K_{I,C} = R_T a_{D,CUR} \qquad (49)$$

so that the closed-loop transfer function becomes

$$\frac{i_R}{i_{R,COM}} = \frac{(\sigma L_R s + R_T) a_{D,CUR}}{(\sigma L_R s + R_T)(s + a_{D,CUR})} = \frac{a_{D,CUR}}{s + a_{D,CUR}} \qquad (50)$$

The closed-loop response is a first-order system with unity gain and a bandwidth specified by $a_{D,CUR}$. Note that a pole is cancelled in the response, but the pole is real and with a negative real part that can be set by choice of the controller parameter R_T.

IV. EXPERIMENTAL RESULTS

A. Hardware platform

The versions of the algorithm with and without current control loop were tested on an experimental platform at the University of Utah. The general organization of the components is shown on Fig. 3. The main elements of the system are a dSPACE DS1104 real-time data acquisition and control system (DAC SYSTEM) hosted by a PC, a Hirel Systems

inverter board (CONVERTER), and a Motorsolver doubly-fed induction machine (M) connected to a Motorsolver brush DC motor (LOAD) whose encoder was used for position measurement (θ). The stator of the DFIM was connected to the three-phase grid through a transformer, lowering the voltage to about 11.1 V_{pk} line-neutral at 60 Hz. The connection was controlled through a relay triggered by a dSPACE digital output.
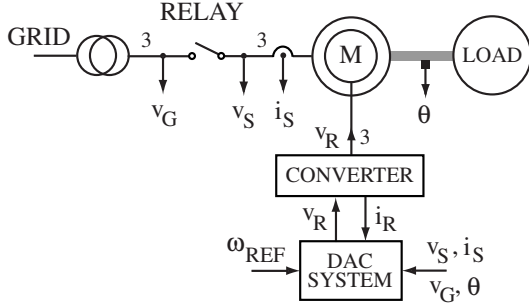

Fig. 3. Organization of the experimental system

The voltages and currents were measured as three-phase variables and converted in the DAC system to the corresponding complex variables using (1) and (3). The line voltages of the grid (v_G) and of the stator (v_S) were measured through voltage reduction networks and the line currents were measured through current sensors. Rotor currents were measured through sensors on the inverter board. The operator could trigger the relay from the PC and apply a reference value for the velocity. For the experiments of the paper, a pre-specified pattern of velocity commands was applied. The command for the stator reactive power was set at zero.

The electrical parameters were estimated through standstill measurements, with the resulting values used in the above example. The inertia was estimated at $J = 3.5 \ 10^{-4}$ kg.m^2. It was found that, for the general purpose platform used, a sampling frequency of 5 kHz was close to the maximum achievable. Accordingly, the bandwidth of the current loop was set at 500 Hz ($a_{D,CUR}$ =3,142 rad/s), and the bandwidth of the velocity loop was set at 50 Hz ($a_{D,VEL}$ =314 rad/s). The same bandwidth was used for the velocity loop in voltage and current command modes.

Before connection to the grid, the algorithm was started with $i_{S,COM} = 0$. The magnitude coefficient m_{adj} was close to 1 in the synchronization phase, and the offset θ_{adj} was adjusted so that the phases of the grid and stator voltages matched. When the phases matched, the relay was engaged with zero torque and reactive power commands. Minimal transients resulted. Then, the speed profiles were applied through the control law.

The controller parameters are given in the table below. The parameter R_T was chosen close to R_R, based on prior simulation experiments. The algorithm also used the variable τ_{LIM}, which was computed in real-time using the actual stator voltages and the smallest value obtained from formulas (30), (32), and (37).

Parameter	Velocity loop			Current loop		
	K_P	K_I	K_F	$K_{P,C}$	$K_{I,C}$	R_T
Value	0.22	34.5	0.67	8.22	3142	1

B. Single motor experiment

A motor was controlled with the voltage command algorithm discussed in the paper with a velocity reference that slowly rose from zero to 2,700 rpm, then was abruptly brought to zero. Fig. 4 shows the speed response of the motor. The reference is also shown but is super-imposed and not distinct at the scale of the plot. With $n_P = 2$, 1,800 rpm is the synchronous speed associated with the 60 Hz grid frequency. Therefore, the plot spans the sub-synchronous and super-synchronous modes, as well as rapid braking of the motor to zero speed.
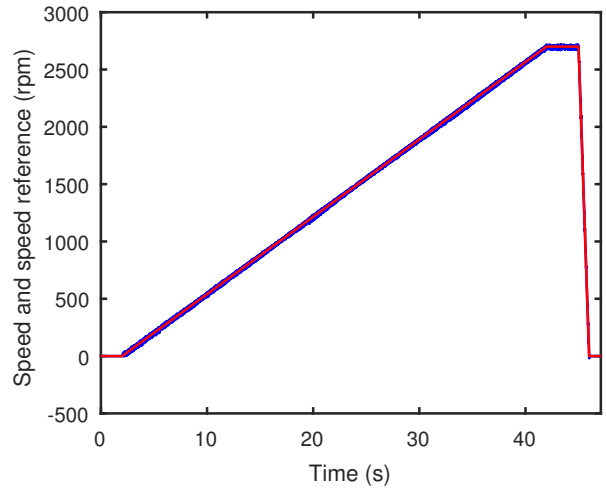

Fig. 4. Speed and speed reference for a linearly increasing speed

Fig. 5 shows the instantaneous values of the stator and rotor peak voltages, using (8) and a similar formula for the rotor voltages but using the magnitude of the complex rotor voltage. Due to the transformer, there is a small variation of the stator voltage. The peak rotor voltage varies significantly with the speed. It is minimized around the synchronous speed, and otherwise increases proportionally to the absolute value of the slip (which can be predicted from (11) and (20)). Fig. 6 shows the instantaneous peak values of the stator and rotor currents, and Fig. 7 shows the rotor currents for the first two phases (X and Y) of the rotor around the synchronous speed. The frequency of the rotor currents becomes small around the synchronous speed. Below the synchronous speed, the rotor currents are in forward sequence, but they switch to the reverse sequence above the synchronous speed.

In the next experiment, a comparison is made between the voltage command and the current command options of the algorithm. A large step of reference velocity was applied at the initial time. Fig. 8 shows the responses with voltage command (VC) and current command (CC), together with the speed reference. Fig. 9 shows the peak rotor current obtained
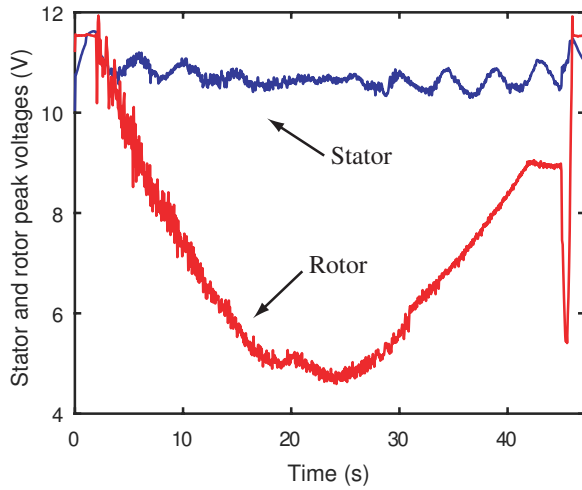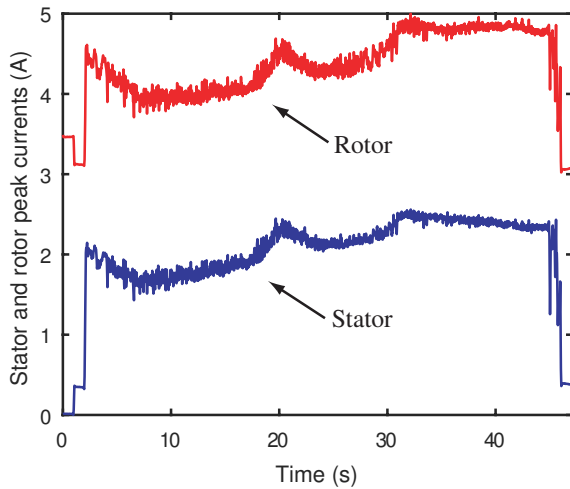
Fig. 5. Peak stator and rotor voltages

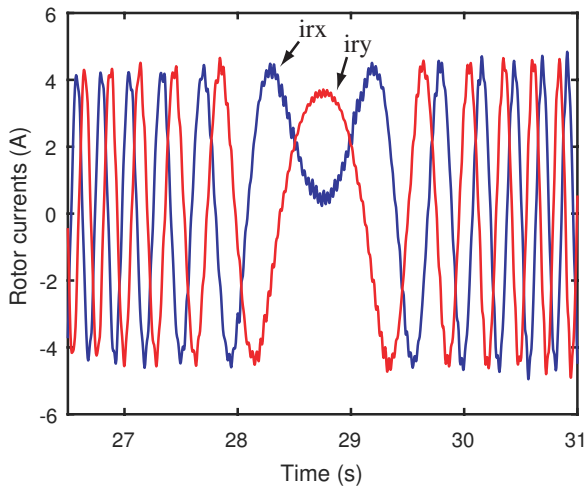Fig. 6. Peak stator and rotor currents

Fig. 7. Rotor currents for phases X and Y around the synchronous speed

with the two options. The plots show that the current command achieves a slightly faster response, while the voltage command results in a small excursion of the peak current over the 6 A limit.
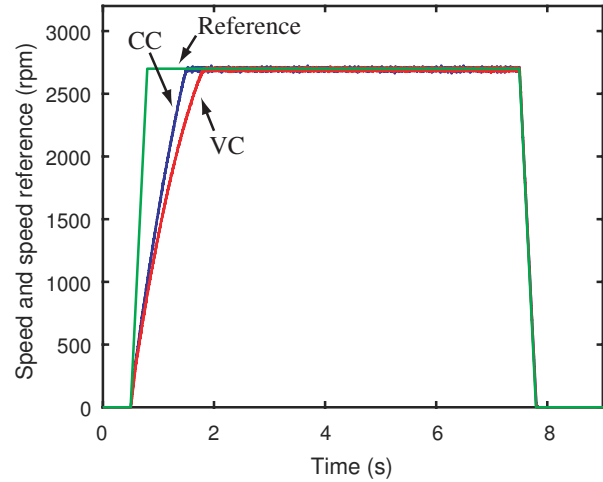

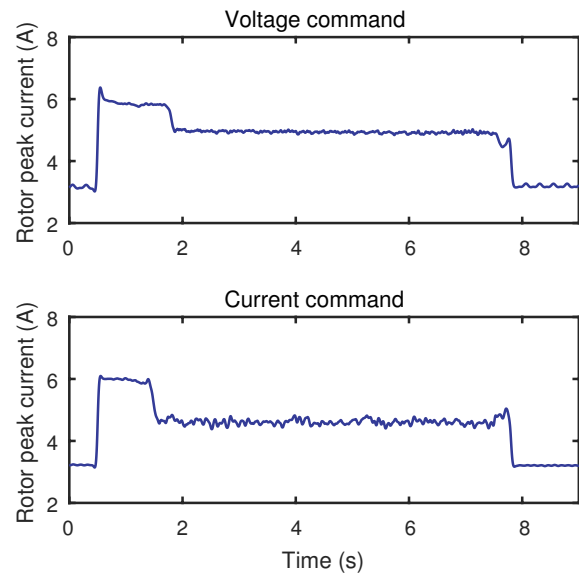Fig. 8. Speed with voltage and current command options for a large step of reference command

Fig. 9. Peak rotor currents with voltage and current command options

The next experiment shows the speed responses with a profile mixing large and small steps. The speed responses, shown in Fig. 10 are very close. The peak rotor current responses shown in Fig. 11 again demonstrate a better respect of the rotor current limit with the current command option. Although lowering the limit could reduce the peak, a better option might be to reduce the rate of variation of the speed reference.
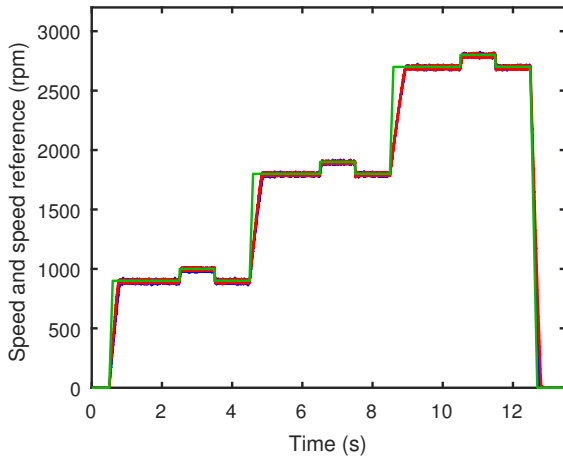
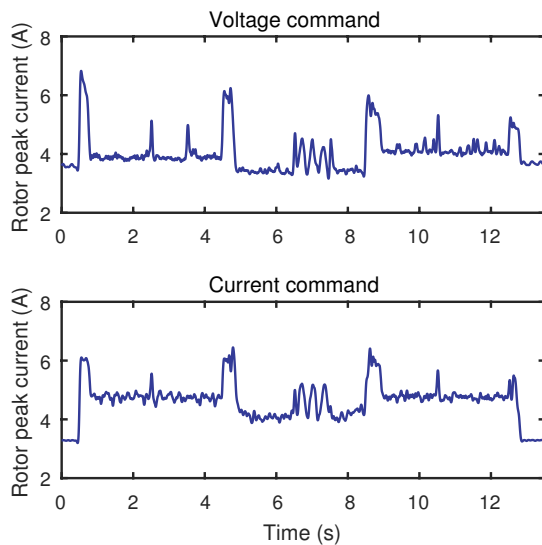Fig. 10. Speed responses for a profile of large and small steps

Fig. 11. Peak rotor current with voltage and current command options for a profile of large and small steps

C. Two motor experiment

The algorithm was also tested with two motors of the same construction connected on the same grid connection and controlled with two copies of the same algorithm. Fig. 12 shows the speed responses of the two motors, which are commanded to reach the synchronous speed (at different times), then to change speed by increments of identical magnitude but opposite sign, then to return to standstill together. The responses follow closely the commands, which are not shown on the plots because they would overlap. Fig. 13 shows the torque commands to the two motors. Interestingly, one motor requires a somewhat lower torque command, possibly due to lower friction in the DC motor used as load. Note that it is possible to successfully control the motors independently despite the common, non-ideal supply. Experiments were also carried out on a similar system at NASA Glenn Research Center, including experiments with three motors in parallel and with a feedback control loop added for the reactive power [12].
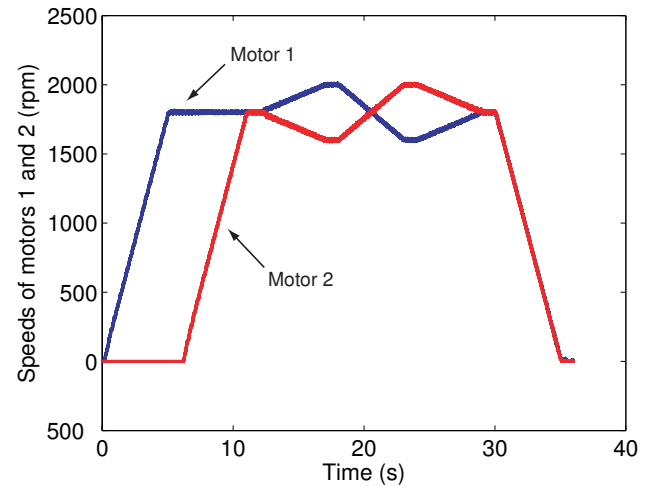

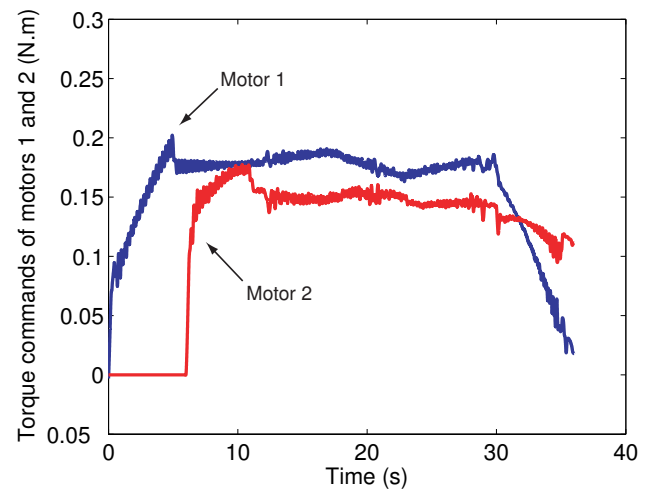Fig. 12. Speed responses of motor 1 and motor 2 for the two-motor experiment

Fig. 13. Torque commands to motor 1 and motor 2 in the two-motor experiment

Overall, excellent results are obtained with remarkably simple algorithms, especially when the voltage command option is used. For illustration, the listing below shows the core Matlab m-code embedded in Simulink to compute the rotor voltages vrx, vry, vrz based on a torque command $tcom$ (assuming $R_S = 0$ and $Q_{S,COM} = 0$). The complex representation involves complex variables instead of the two-dimensional vectors of standard dq transformations. The computations are equivalent, but the complex representation yields a compact representation with few lines of code.

Core control code
a1=[sqrt(2/3) -1/sqrt(6)+1i/sqrt(2) -1/sqrt(6)-1i/sqrt(2)];
a2=a1*[vsa;vsb;vsc];
vs=abs(a2);eithe=a2/vs;
zs=Rs+1i*ome*Ls;zr=Rr+1i*(ome-np*om)*Lr;
zms=1i*ome*M;zmr=1i*(ome-np*om)*M;
vrc=zr*vs/zms-(zs*zr-zms*zmr)*ome*tcom/(zms*vs*np);
a3=vrc*eithe*exp(-1i*np*th);
a4=[sqrt(2/3) 0;-1/sqrt(6) 1/sqrt(2);-1/sqrt(6) -1/sqrt(2)];
vr=a4*[real(a3);imag(a3)];
vrx=vr(1);vry=vr(2);vrz=vr(3);

V. Conclusions

A new algorithm was proposed for the control of doubly-fed induction motors based on voltage commands to a rotor-side converter. Options were presented with and without current feedback. Due to their simplicity, the algorithms are easy to implement and test. The option with current control is slightly more complicated, but provides better tracking and limiting of the peak rotor currents. The voltage command option is useful on its own, but also as an intermediate step for the development of the current command mode. A valuable feature of the algorithms is that the parameters can be selected *a priori* using motor parameters and a reasonable specification for the response time. The core of the control system is an open-loop torque and reactive power control algorithm, which is augmented by an outer PI control loop to regulate the velocity. Limits can be applied to the torque and reactive power commands to avoid exceeding the constraints. These limits can also be computed from machine parameters, and can be adjusted automatically in real-time if some parameters such as the supply voltage or frequency are modified through control of the generator.

VI. Acknowledgements

References

[1] W. Leonhard, *Control of Electrical Drives*, 2nd ed., Springer-Verlag, Berlin, 1996.

[2] I. Boldea, *Variable Speed Generators*, CRC Press, Boca Raton, FL, 2006.

[3] S. Muller, M. Deicke, & R. W. De Doncker, "Doubly Fed Induction Generator Systems for Wind Turbines," *IEEE Industry Applications Magazine,* vol. 8, no. 3, 2002, pp. 26-33.

[4] B. Wu, Y. Lang, N. Zargari, & S. Kouro, *Power Conversion and Control of Wind Energy Systems*, IEEE/Wiley, Hoboken, NJ, 2011.

[5] Y. Liu & L. Xu, "The Dual-Current-Loop Controlled Doubly Fed Induction Motor for EV/HEV Applications," *IEEE Trans. on Energy Conversion*, vol. 28, no. 4, 2013, pp. 1045-1052.

[6] M. Debbou, A. Damdoum, & M. Pietrzak-David, "Optimal Sliding Mode Control for DFIM Electric Marine Thruster," *International Conference on Electrical Systems for Aircraft, Railway, Ship Propulsion and Road Vehicles & International Transportation Electrification Conference (ESARS-ITEC)*, 2016, pp. 1-6.

[7] D. J. Sadey, L. M. Taylor, & R.F. Beach, "Proposal and Development of a High Voltage Variable Frequency Alternating Current Power System for Hybrid Electric Aircraft", *14th International Energy Conversion Engineering Conference*, Salt Lake City, UT, July 2016.

[8] A. Banerjee, M. S. Tomovich, S. B. Leeb, & J. L. Kirtley, "Control Architecture for a Switched Doubly Fed Machine Propulsion Drive," *IEEE Trans. on Industry Applications,* vol. 51, no. 2, pp. 1538-1550.

[9] A. C. Ferreira, L. M. Souza, & E. H. Watanabe, "Improving Power Quality with a Variable Speed Synchronous Condenser," *International Conference on Power Electronics, Machines and Drives*, 2002, pp. 456-461.

[10] L. Morel, H. Godfroid, A. Mirzaian, & J. M. Kauffmann, "Double-fed Induction Machine: Converter Optimisation and Field Oriented Control without Position Sensor," *IEE Proceedings - Electric Power Applications*, vol. 145, no. 4, 1998, pp. 360-368.

[11] S. Peresada, A. Tilli, & A. Tonielli, "Power Control of a Doubly Fed Induction Machine via Output Feedback," *Control Engineering Practice*, vol. 12, no. 1, 2004, pp. 41-57.

[12] D. J. Sadey, M. Bodson, J. T. Csank, K. R. Hunker, C. J. Theman, & L. M. Taylor, "Control Demonstration of Multiple Doubly-Fed Induction Motors for Hybrid Electric Propulsion," *AIAA Propulsion and Energy Forum*, Atlanta, GA, July 2017.

[13] X. Yuan, J. Chai, Y. Li, "A Converter-Based Starting Method and Speed Control of Doubly Fed Induction Machine With Centrifugal Loads," *IEEE Trans. on Industry Applications,* vol. 47, no. 3, 2011, pp. 1409-1418.

[14] Y. Zhang & B. T. Ooi, "Adapting DFIGs for Doubly-Fed Induction Motors Operation," *IEEE Power and Energy Society General Meeting*, 2012, pp 1-8.

[15] J. Zhang, Y. Kang, D.-C. Liao, H-F. Cai, J. Pan, & J. Wu, "Design and Experiment of 155kW Doubly-fed Induction Motor System Used in Pump Stations," *2008 World Automation Congress*, 2008, pp. 1-4.

[16] M. Abdellatiff, M. Debbou, I. Slama-Belkhodja, & M. Pietrzak-David, "Simple Low-Speed Sensorless Dual DTC for Double Fed Induction Machine Drive," *IEEE Trans. on Industrial Electronics,* vol. 61, no. 8, 2014, pp. 3915-3922.

[17] M. Debbou & M. Pietrzak-David, "Novel Tolerant Fault DFIM Drive for Naval Propulsion," *IECON 2013 - 39th Annual Conference of the IEEE Industrial Electronics Society*, 2013, pp. 3006-3011.

[18] G. Poddar & V. T. Ranganathan, "Sensorless Field-Oriented Control for Double-inverter-fed Wound-rotor Induction Motor Drive," *IEEE Trans. on Industrial Electronics*, vol. 51, no. 5, 2004, pp. 1089-1096.

[19] A. M. Knight, R. E. Betz, & D. G. Dorrell, "Design and Analysis of Brushless Doubly Fed Reluctance Machines," *IEEE Trans. on Industry Applications*, vol. 49, no. 1, 2013, pp. 50-58.

[20] L. Xu, B. Guan, H. Liu, L. Gao, & K. Tsai, "Design and Control of a High-Efficiency Doubly-Fed Brushless Machine for Wind Power Generator Application," *IEEE Energy Conversion Congress and Exposition*, 2010, pp. 2409-2416.

[21] P. Han, M. Cheng, & Z. Chen, "Single-Electrical-Port Control of Cascaded Doubly-Fed Induction Machine for EV/HEV Applications," *IEEE Trans. on Power Electronics*, vol. 32, no. 9, 2017, pp. 7233-7243.

[22] Y. H. Ku, "Transient Analysis of Rotating Machines and Stationary Networks by Means of Rotating Reference Frames," *Trans. of the American Institute of Electrical Engineers*, vol. 70 , no. 1, 1951, pp. 943-957.

[23] D.W. Novotny & J.H. Wouterse, "Induction Machine Transfer Functions and Dynamic Response by Means of Complex Time Variables," *IEEE Trans. on Power Apparatus and Systems*, vol. 95 , no. 4, 1976, pp. 1325-1335.

[24] M. Bodson, "Design of Controllers in the Complex Domain," *IEEE Conference of Decision and Control*, Los Angeles, CA, 2014, pp. 4077-4082.

[25] A. Dòria-Cerezo, M. Bodson, C. Batlle, & R. Ortega, "Study of the Stability of a Direct Stator Current Controller for a Doubly Fed Induction Machine Using the Complex Hurwitz Test," *IEEE Trans. on Control Systems Technology*, vol. 21, no. 6, 2013, pp. 2323-2331.

[26] N. Mohan, *Advanced Electric Drives*, Wiley, Hoboken, NJ, 2014.

[27] H. Baesmat & M. Bodson, "Design of Pole Placement Controllers for Doubly-Fed Induction Generators in the Complex Domain," *2015 IEEE Power & Energy Society General Meeting*, Denver, CO, 2015, pp. 1-5.

[28] H. Baesmat & M. Bodson, "Pole Placement Control for Doubly-Fed Induction Generators Using Compact Representations in Complex Variables," to appear in *IEEE Trans. on Energy Conversion*, available with early access, 2018.

[29] A. Dòria-Cerezo & M. Bodson, "Design of Controllers for Electrical Power Systems Using a Complex Root Locus Method," *IEEE Trans. on Industrial Electronics*, vol. 63, no. 6, 2016, pp. 3706-3716.

[30] M. Bodson & O. Kiselychnyk, "The Complex Hurwitz Test for the Analysis of Spontaneous Self-Excitation in Induction Generators," *IEEE Trans. on Automatic Control*, vol. 58, no. 2, pp. 449-454, 2013.

[31] D. W. Novotny & T. A. Lipo, *Vector Control and Dynamics of AC Drives*, Oxford University Press, NY, 1996.

[32] F. B. del Blanco, M. W. Degner, & R. D. Lorenz, "Dynamic Analysis of Current Regulators for AC Motors Using Complex Vectors," *IEEE Trans. on Industry Applications*, vol. 35, no. 6, 1999, pp. 1424-1432.

[33] S.-K. Sul, *Control of Electric Machine Drive Systems*, Wiley, Hoboken, NJ, 2011.